ADVANCED MATERIALS
www.advmat.de

Check for updates

Machine Learning Guided Synthesis of Flash Graphene

*Jacob L. Beckham, Kevin M. Wyss, Yunchao Xie, Emily A. McHugh, John Tianci Li, Paul A. Advincula, Weiyin Chen, Jian Lin, and James M. Tour**

Advances in nanoscience have enabled the synthesis of nanomaterials, such as graphene, from low-value or waste materials through flash Joule heating. Though this capability is promising, the complex and entangled variables that govern nanocrystal formation in the Joule heating process remain poorly understood. In this work, machine learning (ML) models are constructed to explore the factors that drive the transformation of amorphous carbon into graphene nanocrystals during flash Joule heating. An XGBoost regression model of crystallinity achieves an r^2 score of 0.8051 ± 0.054. Feature importance assays and decision trees extracted from these models reveal key considerations in the selection of starting materials and the role of stochastic current fluctuations in flash Joule heating synthesis. Furthermore, partial dependence analyses demonstrate the importance of charge and current density as predictors of crystallinity, implying a progression from reaction-limited to diffusion-limited kinetics as flash Joule heating parameters change. Finally, a practical application of the ML models is shown by using Bayesian meta-learning algorithms to automatically improve bulk crystallinity over many Joule heating reactions. These results illustrate the power of ML as a tool to analyze complex nanomanufacturing processes and enable the synthesis of 2D crystals with desirable properties by flash Joule heating.

1. Introduction

The scalable synthesis of nanomaterials is a crucial goal in materials science. To achieve the widespread use of nanotechnology, nanomaterials must be synthesized by rapid and scalable processes that do not deleteriously affect their properties. To address this challenge, we and others recently reported the synthesis of graphene,[1–3] as well as mixed-phase MoS_2 and WS_2,[4] high-entropy alloy NPs,[5,6] nanodiamond,[7] and other nanomaterials using the electrothermal flash Joule heating effect. The graphene product was called "flash graphene" after the intense black body radiation produced during the electrical discharge. Flash Joule heating permits the conversion of amorphous carbon, including waste such as pyrolyzed rubber tires,[8] ash by-products from plastic recycling,[9] or landfill-grade mixed plastic waste,[10] into graphene crystals. Furthermore, flash graphene crystals are turbostratic and exhibit varying degrees of layer-to-layer misorientation along the *c*-axis.[1] Such turbostratic graphene possesses nanostructure-dependent properties, including enhanced solubility in surfactant solutions[1] and altered band structure.[11] The scalable and environmentally friendly nature of the Joule heating process, as well as the turbostratic nature of the synthesized product, make flash Joule heating an intriguing synthetic technique that warrants further study and analysis.

Although flash Joule heating has immense practical utility, it is intrinsically difficult to study. The flash graphene formation process occurs in just hundreds of milliseconds. Furthermore, present-day flash Joule heating reactors do not offer control over the current discharge profile, adding a stochastic element to each reaction that depends on momentary fluctuations in circuit-to-sample contact. These fluctuations are difficult to control experimentally, making it challenging to map process–structure–property relationships by a traditional grid-search. Due to these factors, the parameters that drive bulk nanocrystal formation during flash Joule heating remain ambiguous.

At the same time, an emerging body of literature indicates that machine learning (ML) is a powerful tool for fundamental studies in materials science.[12–18] While ML is classically considered an industrial tool for process failure prevention, the use of ML to interrogate large parameter spaces can yield insights on new technologies at a low time-cost. For example, Tang et al. used ML to explore the process–structure–property relationships governing well-understood processes, such as chemical vapor deposition and quantum dot synthesis, and argued based on their results that ML would allow researchers to investigate

J. L. Beckham, K. M. Wyss, E. A. McHugh, J. T. Li, P. A. Advincula, W. Chen
Department of Chemistry
Rice University
6100 Main Street MS 222, Houston, TX 77005, USA
Y. Xie, J. Lin
Department of Mechanical and Aerospace Engineering
University of Missouri
Columbia, MO 65211, USA
J. M. Tour
Department of Chemistry
Smalley-Curl Institute
NanoCarbon Center
Welch Institute for Advanced Materials
Department of Materials Science and Nanoengineering
Department of Computer Science
Rice University
6100 Main Street MS 222, Houston, TX 77005, USA
E-mail: tour@rice.edu

The ORCID identification number(s) for the author(s) of this article can be found under https://doi.org/10.1002/adma.202106506.

DOI: 10.1002/adma.202106506

© 2022 Wiley-VCH GmbH

15214095, 2022, 12, Downloaded from https://onlinelibrary.wiley.com/doi/10.1002/adma.202106506 by Shanxi University, Wiley Online Library on [23/01/2024]. See the Terms and Conditions (https://onlinelibrary.wiley.com/terms-and-conditions) on Wiley Online Library for rules of use; OA articles are governed by the applicable Creative Commons License

them more efficiently than was previously possible.[16] This work is emblematic of a growing acknowledgement that ML possesses tremendous potential even in exploratory research.

Immense progress has been made by utilizing ML in materials engineering,[19] especially in theoretical studies,[20,21] where ML is commonly used to approximate solutions to partial differential equations and enhance predictions of materials properties. These ML-enhanced property predictions can then serve to identify promising candidate materials.[22] Furthermore, Bayesian model-based optimization techniques offer new avenues for materials discovery and property improvement.[23,24] Such optimization techniques leverage ML's propensity for function approximation to minimize or maximize a given objective function, in many cases opening new opportunities for automated materials processing. In previous studies, Bayesian optimization algorithms were used to design shape-tailored gold nanocrystals,[25] optimize composite designs for various force-loading conditions,[26] and uncover novel syntheses for organic compounds.[27] Some Bayesian learning algorithms have even been designed specifically for scientific exploration, using boundary-free methods to facilitate identification of out-of-trend observations in high-throughput computational studies.[28]

Here, we construct ML models to predict the effects of flash Joule heating process parameters on the crystallization of flash graphene from low-value materials or waste. The unique capabilities of ML enable a detailed study of direct-current flash Joule heating despite the large parameter space involved and the presence of uncontrollable stochastic elements. Furthermore, we demonstrate the use of a Bayesian optimization algorithm to iteratively improve graphene crystallization over many trials. These results offer useful insights regarding the flash Joule heating technique and provide a potent demonstration showing how ML can enhance the study of new materials synthesis technologies.

2. Results and Discussion

As shown in **Figure 1**a, we first synthesized flash graphene from four low-to-negative value amorphous carbon starting materials in $N = 173$ separate Joule heating reactions. Flash Joule heating was performed on a custom-built direct-current Joule heating station (Figure S1, Supporting Information). The starting materials employed in these reactions were: carbon black,[1] plastic waste-derived pyrolysis ash,[9] pyrolyzed rubber tires,[8] and metallurgical coke. Then, we assessed the structural character of each sample by wide-area Raman mapping. Each of the >20 000 spectra collected in this study was preprocessed (Figure S2, Supporting Information) and analyzed by custom-written scripts, which compiled a metric to estimate the proportion of the amorphous starting material in each sample that had crystallized into graphene. This metric was termed the "graphene yield." Finally, we constructed a suite of ML models to predict the graphene yield of each reaction.

Sample Raman spectra of amorphous carbon, graphene, and highly turbostratic graphene are shown in Figure 1b. Raman spectroscopy is a powerful technique for the structural characterization of carbon, especially graphitic materials.[29–31] Spectra of amorphous carbon contain two bands: the G and D bands. The D band is forbidden by selection rules, but it commonly appears due to symmetry disruptions, such as armchair edges or point defects. Raman spectra of graphene and graphite contain the second-order overtone of the D band, referred to as the 2D band. The appearance of this band is a positive indicator for the formation of a graphitic lattice, and its shape and intensity offer important nanostructural information. Spectra of high-quality turbostratic flash graphene contain a resonance-enhanced single-Lorentzian 2D band with a narrow full-width at half-maximum (FWHM; ≈16 cm^{-1}) and a magnified I_{2D}/I_G peak intensity ratio (up to a maximum of 17) as compared to pristine single-layer graphene (which possesses I_{2D}/I_G of ≈3).[32]

Histograms in Figure 1c–f show sample-level statistics compiled from Raman mapping, including the graphene yield, the average I_{2D}/I_G, the average I_D/I_G, and the average FWHM of the 2D band. Statistics on individual spectra (shown in Figure 1g–i) illustrate relationships between the I_{2D}/I_G ratio, the FWHM of the 2D band, and the position of the 2D band, showing a blue-shifted and narrowed 2D band at high I_{2D}/I_G which is indicative of resonance-enhanced turbostratic graphene.[2,10,32] Wide-area mapping is used to assess crystallinity because the Raman spectra of flash graphene samples can vary quite widely throughout individual samples (Figure S3, Supporting Information). The high-throughput nature of the mapping assay ensures that the compiled metric accurately captures the bulk character of each sample. From these mapping assays, the "graphene yield" can then be calculated as the percentage of Raman spectra from each sample that can be classified as graphene rather than amorphous carbon (a detailed discussion of selection criteria can be found in the Experimental Section). This graphene yield metric was then validated quantitatively by thermogravimetric analysis and qualitatively by scanning electron microscopy. Thermograms show that higher-yield flash graphene samples were typically more thermally stable than their lower-yield counterparts (Figure S4, Supporting Information), while scanning electron micrographs reveal a visible microstructural evolution from low-to-high crystallinity (Figure S5, Supporting Information). Flashed materials were additionally characterized by X-ray diffraction (XRD; Figure S6, Supporting Information) and X-ray photoelectron spectroscopy (Figures S7–S10 and Table S1, Supporting Information).

2.1. Model Construction and Performance

ML regression models were constructed to predict the graphene yield metric derived from Raman spectral mapping. First, a total of five features were empirically selected from the available parameters tested for the prediction of graphene yield (see Table S2 and Figures S11–S14 in the Supporting Information for a summary of the features attempted and dataset characteristics). Then, the five selected features were then used to train six ML regression models for the prediction of graphene yield. Linear regression (LR-R),[33] Bayesian regression (BR-R),[34] multilayer perceptron (MLP-R),[35] decision tree (DT-R),[36] random forest (RF-R),[37] and eXtreme Gradient Boosting (XGB-R)[38] regression models were trained using fivefold cross-validation. Hyperparameters were tabulated in Table S3 in the Supporting Information.

15214095, 2022, 12, Downloaded from https://onlinelibrary.wiley.com/doi/10.1002/adma.202106506 by Shanxi University, Wiley Online Library on [23/01/2024]. See the Terms and Conditions (https://onlinelibrary.wiley.com/terms-and-conditions) on Wiley Online Library for rules of use; OA articles are governed by the applicable Creative Commons License

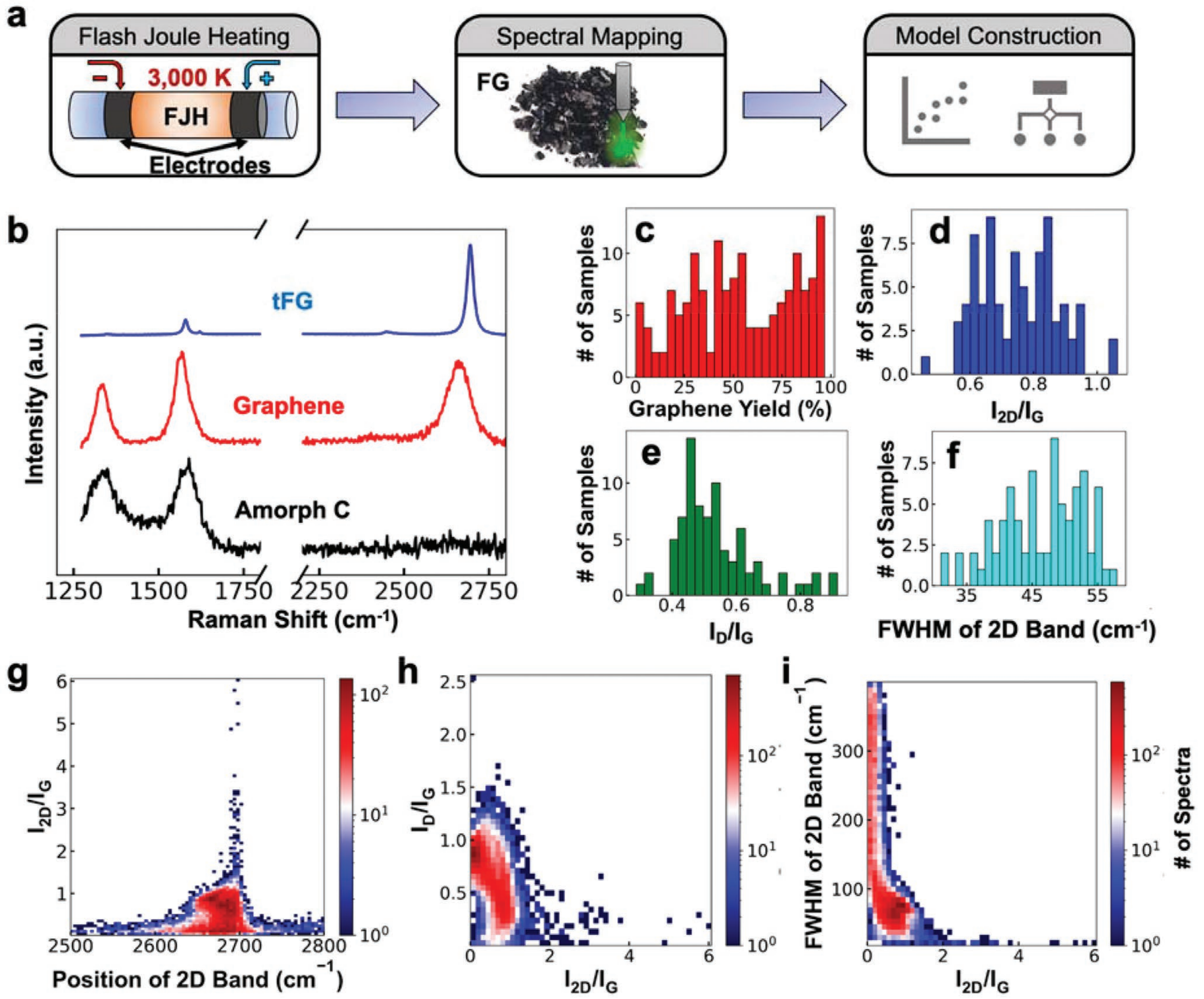

Figure 1. Scheme and analysis of dataset. a) Schematic depiction of study. b) Sample Raman spectra of amorphous carbon, graphene, and turbostratic flash graphene, exemplifying the distinction between typical flash graphene spectra (red) and spectra from highly turbostratic graphene crystals (blue). These Raman spectra were collected from flashed samples of carbon black. c–f) Bulk average statistics of the graphene yield, I_{2D}/I_G, I_D/I_G, and FWHM of the 2D band of each sample analyzed in this study. g–i) 2D histograms showing statistics from ≈16 000 Raman spectra obtained from spots of flash Joule heated material, showing relationships between g) the 2D band position and I_{2D}/I_G, h) I_{2D}/I_G and I_D/I_G, and i) I_{2D}/I_G and the FWHM of the 2D band. These plots show the blue shift, narrowing, and resonance enhancement of the 2D band in spectra from highly turbostratic graphene crystals.

Figure 2a,b shows the performance of regression models predicting graphene yield. For this task, decision tree-based models, including DT-R, RF-R, and XGB-R, achieved the best performance. RF-R models achieved root mean squared error (RMSE) of 12.7% ± 1.3% and an r^2 score of 0.7808 ± 0.064. XGB-R models, such as the example shown in Figure 2c, achieved even better performance, with an RMSE of 11.3% ± 2.2% and an r^2 score of 0.8051 ± 0.054. The error distribution was skewed, as ≈40% of the samples tested showed predictions that were <5% off from the true value (Figure 2d). Sample performances of other ML regression models are shown in Figure S15 in the Supporting Information.

ML models arrive at their predictions based on the algorithms upon which they are constructed. Decision tree-based models, i.e., DT-R, RF-R, and XGB-R, make predictions based on a series of if/then statements derived from the input features, which together form a "tree" of many branches that yield different predictions of the output metric. The DT-R model uses a single decision tree, while the RF-R model uses an ensemble of trees to produce a weighted average prediction. The XGB-R model also uses an ensemble of trees, but it constructs trees and sequentially weights their prediction. This sequential weighting, called "gradient boosting," enhances model accuracy and has led XGB-R to be one of the most widely used ML models since its introduction in 2016.[17,38,39] In contrast to decision tree-based models, linear regression models, such as LR-R and BR-R, make predictions based on linear combinations of the input features. Decision trees systematically outperform linear models in this study, suggesting that the relationships between crystallinity and the input

© 2022 Wiley-VCH GmbH

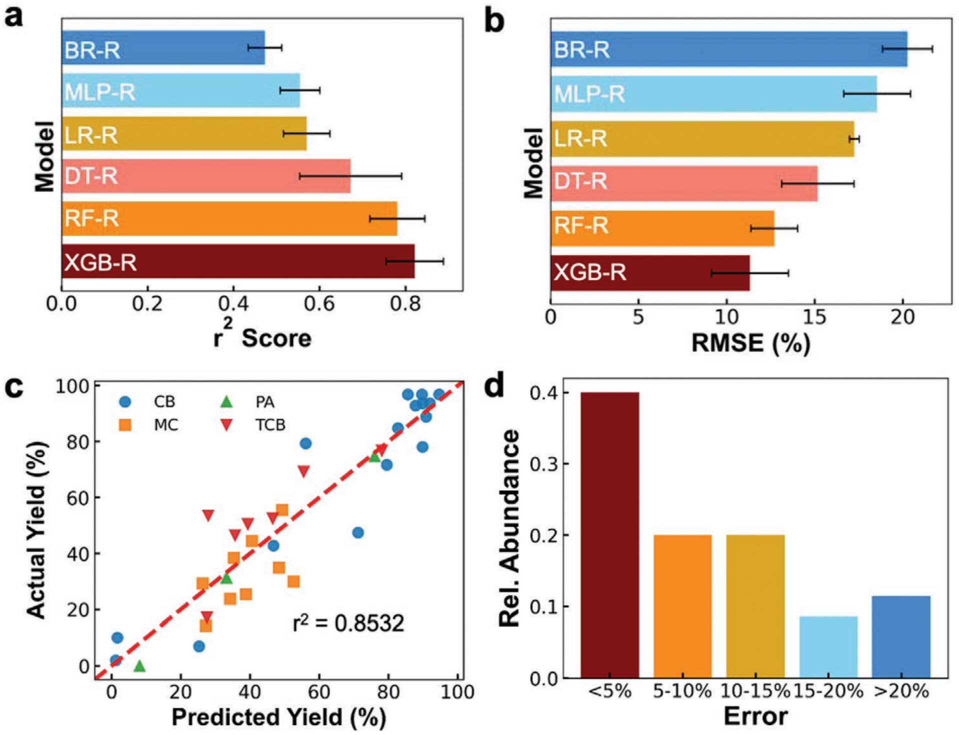

Figure 2. Performance of regression models predicting graphene yield. a) Typical r^2 scores of six types of regression models for the prediction of graphene yield from flash parameters. Error bars represent the standard deviation of the r^2 scores across five train/test split iterations. b) RMSE of the six models presented in (a). c) Performance of an XGB-R for the prediction of graphene yield. CB: carbon black; PA: pyrolysis ash; MC: metallurgical coke; TCB: tire-derived carbon black. d) A typical error distribution for an XGB-R model of graphene yield.

parameters used to train the model are nonlinear (Figure S16, Supporting Information).[40] An artificial neural network (MLP-R) also achieves satisfactory predictions of crystallinity, but is outperformed by the decision tree-based models in this study.

2.2. Model Interpretation and Analysis

2.2.1. Feature Importance Analysis

Feature importance analysis provides an estimate of the predictive power of all the features used to train an ML model. **Figure 3** introduces the features used to train ML models predicting crystallization. The selected features were the charge density (CD), the material type (M), the area under the time–current curve divided by the sample mass (A_{IT}), the maximum current divided by the sample mass (I_{Max}), and the final current divided by the maximum current ($I_{\mathrm{F}}/I_{\mathrm{Max}}$). Two of the features, CD and M, were derived from controllable flash Joule heating experimental variables. The other three features, A_{IT}, I_{Max}, and $I_{\mathrm{F}}/I_{\mathrm{Max}}$, were derived from time–current curves recorded during the reaction by a Hall effect sensor (Figure 3a) and extracted using custom-written scripts. While predictions of crystallinity could be made with the experimental parameters alone, the time–current curves offered complementary information regarding changes in the sample resistance over time, as well as fluctuations in contact between the sample and the circuit due to outgassing. These changes are difficult to control experimentally. Consequently, the inclusion of current-derived statistics in the feature set boosted model performance (Table S2, Supporting Information). Figure 3b shows the correlation matrix between the five empirically selected features.

Figure 3c shows a feature importance analysis for the features used to train the XGB-R model, which indicates that CD was the most crucial feature for predictions of bulk crystallinity. CD represents the amount of charge inside the flash Joule heating station's capacitor bank at $t = 0$ per g of carbon. It is calculated by multiplying the initial voltage (V_0) by the capacitance of the system (C) and dividing by the sample mass (m). Since Joule heating produces thermal energy from collisions between electrons and atomic nuclei,[41] CD is likely related to heat or energy density. Previously, charge and current density were found to control the rate of transformations of carbon materials on smaller scales.[42,43] Moreover, prior experiments in other nonequilibrium graphene synthesis techniques showed that laser-induced graphene synthesis depended on the reaction reaching a critical irradiation fluence to achieve sufficient energy density.[44] Figure 3d shows that, generally, flash Joule heating reactions with low CD produce fewer graphene crystals, while most flash Joule heating reactions with high yield employ high CD. Decision trees extracted from the XGB-R model further support the hypothesis that high CD leads to high yield predictions (Figure 3e). Figure S17 in the Supporting Information explores the relationship between CD and graphene yield, showing that the specific combination of C, V_0, and m into CD produces a metric that is more correlated with crystallinity.

The chosen starting material, denoted "M," also plays a critical role in predicting flash Joule heating efficacy as shown in Figure 3c. This is also apparent from Figure 2c, which shows

15214095, 2022, 12, Downloaded from https://onlinelibrary.wiley.com/doi/10.1002/adma.202106506 by Shanxi University, Wiley Online Library on [23/01/2024]. See the Terms and Conditions (https://onlinelibrary.wiley.com/terms-and-conditions) on Wiley Online Library for rules of use; OA articles are governed by the applicable Creative Commons License

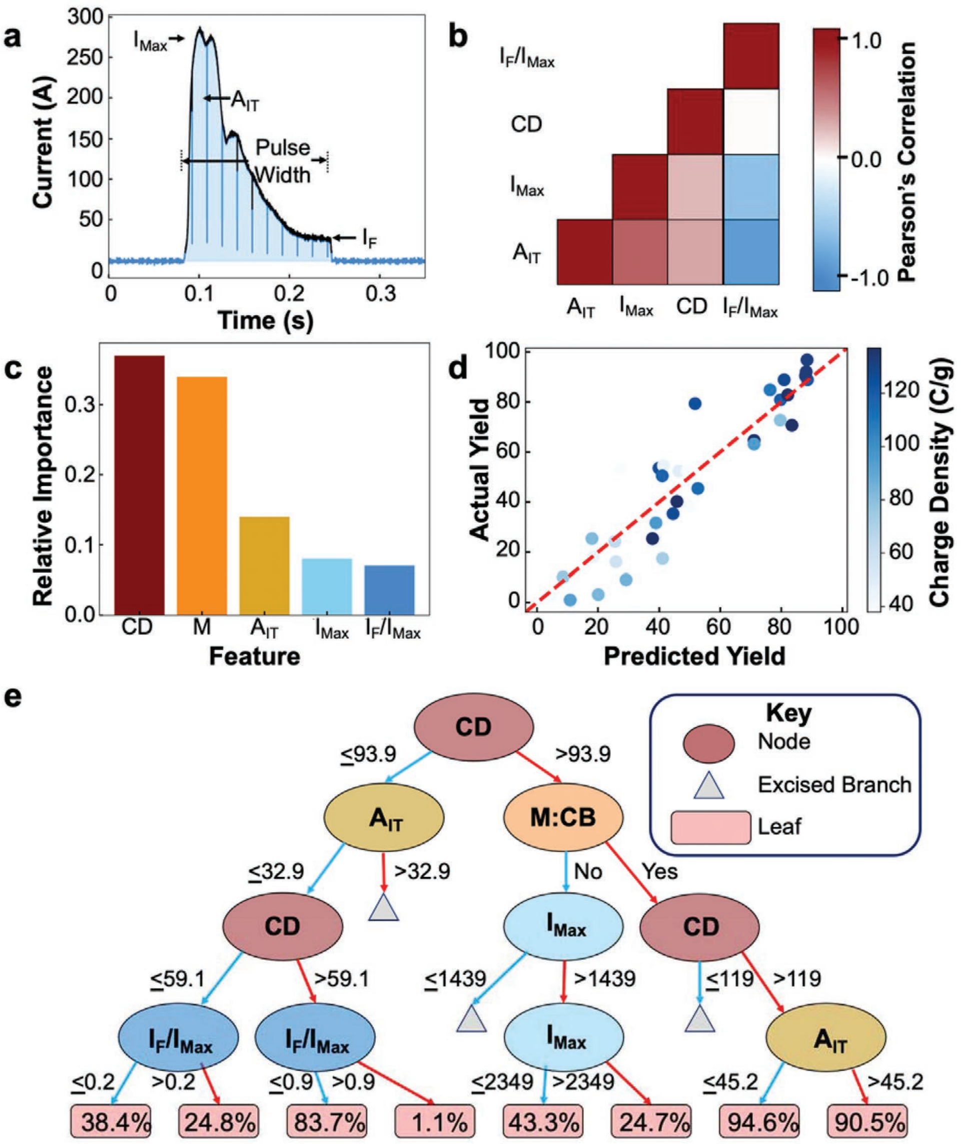

Figure 3. Feature analysis of XGB-R model for prediction of graphene yield. a) A sample time–current curve showing features extracted from the discharge profile of each flash. b) A correlation map of the five features used to train ML models. c) Relative feature importance of the five empirically chosen features included in this model. d) Color map of the graphene yield prediction of the test data set after train/test splitting and training of the model on the training data. The color map illustrates the effect of charge density on the predicted and actual yields. e) Map of a typical decision tree derived from XGB-R showing the effects of various process parameters on the final predicted value. Individual decision trees are weighted according to their accuracy to assemble a final prediction value. CD: charge density; M: material type; A_{IT}: area under the time–current curve normalized to the sample mass; I_{Max}: maximum current normalized to the sample mass; I_F/I_{Max}: final current divided by maximum current.

that, generally, carbon black-derived flash graphene possessed high crystallinity, while metallurgical coke-derived flash graphene possessed low crystallinity even in conditions of high CD. This precursor-dependent crystallization likely cannot be attributed to differential heating abilities, as the low resistance of metallurgical coke allows the generation of higher current compared to the other three feedstocks (Figure S18, Supporting Information). Therefore, the lower crystallinity of coke-derived flash graphene likely arises from the large size of the metallurgical coke particles (150–210 µm).

The other three features, i.e., A_{IT}, I_{Max}, and I_F/I_{Max}, make smaller but still significant contributions to model predictions of graphene yield. A_{IT} is the area under the time–current curve divided by the mass, while I_{Max} is the peak current divided by the mass. Ergo, three of the five features used to train the model, CD, A_{IT}, and I_{Max}, represent metrics of charge or current density. CD and A_{IT} are conceptually similar, both representing measurements of charge per unit mass, but they convey different information and are not correlated ($r = 0.36$). CD, which is calculated using the initial voltage V_0, represents the charge present in the capacitors at $t = 0$. Conversely, A_{IT} represents the charge that passes through the sample during the reaction, which relates to the voltage drop ΔV rather than V_0. As a result, CD offers information about the initial state

15214095, 2022, 12, Downloaded from https://onlinelibrary.wiley.com/doi/10.1002/adma.202106506 by Shanxi University, Wiley Online Library on [23/01/2024]. See the Terms and Conditions (https://onlinelibrary.wiley.com/terms-and-conditions) on Wiley Online Library for rules of use; OA articles are governed by the applicable Creative Commons License

of the system, while A_{IT} offers information about the system while the reaction is taking place. The large dependence of graphene yield on CD might indicate that most of the crystallization reaction occurs near the beginning of the flash Joule heating reaction, which has previously been predicted theoretically.[1] Alternatively, the lack of a neat dependence on the Joule-Lenz power, which scales with V_0^2 rather than V_0 (Table S2, Supporting Information), could offer evidence that electrostatic effects[41] contribute in tandem with Joule heating to the formation of large flash graphene crystals.[45] Nevertheless, the predictive power of CD, A_{IT}, and I_{Max} suggests that charge and current density are the key considerations in the prediction of flash Joule heating reaction efficacy. Finally, $I_{\mathrm{F}}/I_{\mathrm{Max}}$ likely conveys whether the reaction was forced to stop prematurely due to stochastic contact disruptions or outgassing.

2.2.2. Partial Dependence Analysis

Partial dependence (PD) analysis is a powerful analytical tool accessible through ML. PD represents the average model prediction for given values of each feature. Partial dependence plots (PDPs) map relationships between features and the target output, giving additional insight as to how ML models arrive at their conclusion. For example, PDPs from decision tree models show sharp dips and wrinkles at the nodes of prominent trees, whereas PDPs from other models show a smoother PD surface (Figures S19 and S20, Supporting Information). Multivariable PDPs of the quantitative features included in the XGB-R model are shown in **Figure 4**. They reveal that the three metrics related to charge or current density (CD, A_{IT}, and I_{Max}) have similar relationships with crystallinity. At low values of "x," graphene yield systematically increases with the values of these features. Then, at higher values, this relationship plateaus.

Justification for the behavior observed in PD functions of CD, A_{IT}, and I_{Max} can be found by taking inspiration from wet nanocrystal synthesis. Since charge or current in flash Joule heating is related to energy density, increasing the values of these metrics is analogous to increasing the temperature in a classical synthesis reaction. Following this analogy, such a dynamic relationship between energy density and crystallinity could suggest a shift in reaction kinetics from surface reaction-controlled nucleation to a diffusion-controlled regime.[46] At low reaction energies, nucleation occurs selectively at hotspots, and increasing the energy density can dramatically affect the bulk crystallinity of the product. However, at higher reaction energies, the entire sample volume receives sufficient energy for nucleation. In this regime, increasing the reaction energy no longer affects the crystallinity of the end-product (Figure S21, Supporting Information). The PDPs shown in Figure 4 suggest that such a transition may occur at CD values between 100 and 120 C g^{-1} where PD ceases to increase with CD. Consequently, this range might serve as useful benchmarks for new flash Joule heating syntheses or systems. Additionally, it is possible

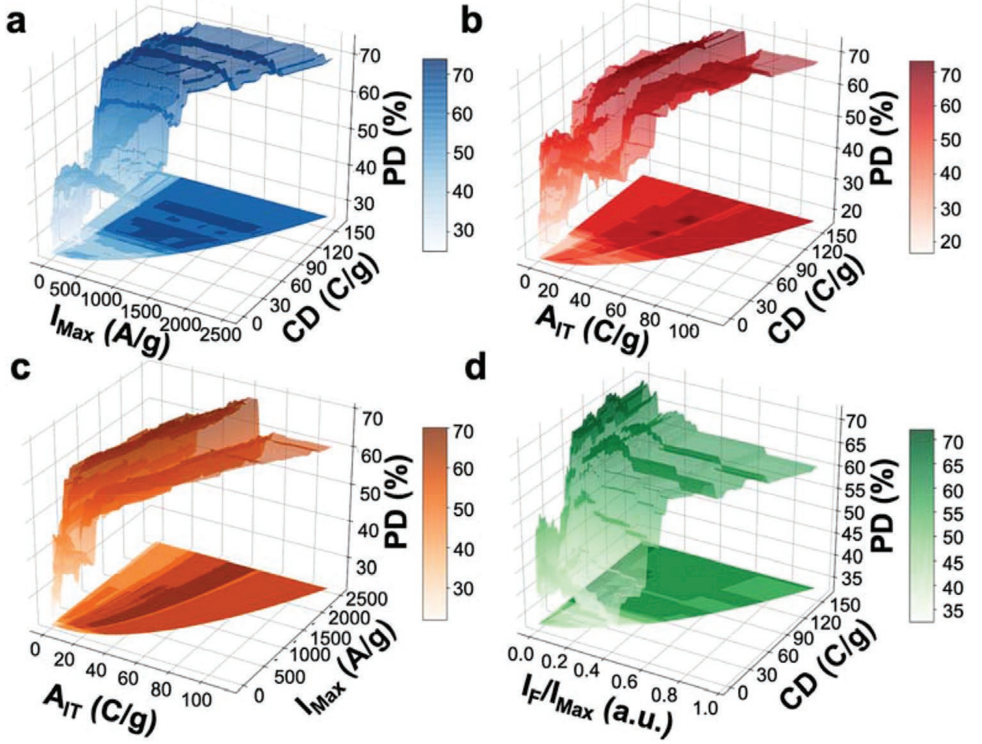

Figure 4. Multivariable partial dependence plots (PDPs) of a) charge density and normalized maximum current, b) charge density and normalized area under the current/time curve, c) normalized maximum current and area under the current/time curve, and d) charge density and the final current divided by the maximum current. PDPs were constructed based on the predictions of models for samples in the test data set. Each plot maps PD (on the z-axis) for given values of two features (on the x- and y-axis). The color map overlaid on the xy-grid reflects the value of PD as a function of the two chosen features and serves as a visual aid.

© 2022 Wiley-VCH GmbH

15214095, 2022, 12, Downloaded from https://onlinelibrary.wiley.com/doi/10.1002/adma.202106506 by Shanxi University, Wiley Online Library on [23/01/2024]. See the Terms and Conditions (https://onlinelibrary.wiley.com/terms-and-conditions) on Wiley Online Library for rules of use; OA articles are governed by the applicable Creative Commons License

15214095, 2022, 12, Downloaded from https://onlinelibrary.wiley.com/doi/10.1002/adma.202106506 by Shanxi University, Wiley Online Library on [23/01/2024]. See the Terms and Conditions (https://onlinelibrary.wiley.com/terms-and-conditions) on Wiley Online Library for rules of use; OA articles are governed by the applicable Creative Commons License

that increasing the flash Joule heating reaction energy beyond this transition point would move the nucleation process further into the realm of diffusion control, causing disperse nucleation and allowing some degree of size control over flash graphene crystals.

2.3. Bayesian Optimization

The previous analyses show ML's ability to derive process–structure–property relationships in flash Joule heating synthesis. However, from a practical point of view, it is vital that these relationships can guide new syntheses using the knowledge they provide. Therefore, we sought to use ML predictions of flash graphene crystallinity to recommend synthesis reaction conditions for new feedstocks using Bayesian model-based optimization (**Scheme 1**). First, a "starter" data set compiled using randomly generated parameters was fed to the algorithm. Then, the algorithm generated predictions based on an RF-R surrogate model and suggested a new set of parameters. The algorithm leverages experience from past trials to explore the parameter space, trading off expected performance and exploration of uncertainty according to an assigned acquisition function.[24,47] Eventually, this exploration yielded an enhanced graphene yield. Altogether, this automation process results in a system that can robustly synthesize flash graphene from waste with no prior knowledge about the starting material.

Toward this end, we implemented the process in Scheme 1 using pyrolyzed rubber tires as a model waste material. **Figure 5**a,b shows that, after just 30 iterations, the mean graphene yield of tire carbon black-derived flash graphene synthesized using parameters suggested by the Bayesian optimization algorithm is 79%. This is significantly ($p < 0.0001$) higher than that achieved by random parameter values (36%). The improvement of crystallization efficacy throughout the optimization process is additionally verified by XRD analysis (Figure S22, Supporting Information) and scanning electron microscopy (Figure S23, Supporting Information). Figure 5c shows that the improvements in flash graphene crystallinity depend on the identification of a favorable region in the flash Joule heating parameter space, with an optimal pretreatment, mass, pulse width, and charge density. Figure 5d–i shows PD relationships derived from the RF-R model used to suggest new parameters. The relationships derived from the learner model are consistent with findings from the full dataset, as prediction values show direct correlations to voltage and capacitance but inverse correlations to sample mass.

The efficacy of the Bayesian optimization algorithm offers a promising outlook for automated flash graphene synthesis. Since flash graphene is commonly synthesized from waste materials,[1,8–10] advantageous precursors for flash Joule heating are diverse and likely to continually evolve as new exploitable wastes are identified for upcycling. Furthermore, many waste streams, such as those derived from household waste, will likely possess a high degree of heterogeneity. Therefore, it is vital to be able to readily synthesize flash graphene from scratch with new starting materials and processes. The Bayesian optimization algorithm demonstrated here shows the ability to take waste materials with no prior identification or characterization and produce high-quality flash graphene in a low number of trials. Further development of this technique, potentially including the use of principal component analysis to process the Raman spectral profile of the produced graphene more directly,[48] may streamline the flash Joule heating process even further and lead to higher accuracy in optimization. These results show the capability of ML to accelerate the synthesis of nanomaterials by flash Joule heating.

3. Conclusion

This study provides a framework for the use of ML to predict the efficacy of flash Joule heating reactions in nanomaterial synthesis. ML models have been used to predict the extent of crystal formation, extract fundamental information, and drive process optimization. Feature analyses from these models showed that metrics of charge and current density primarily dictated the extent of crystallization. Furthermore, the

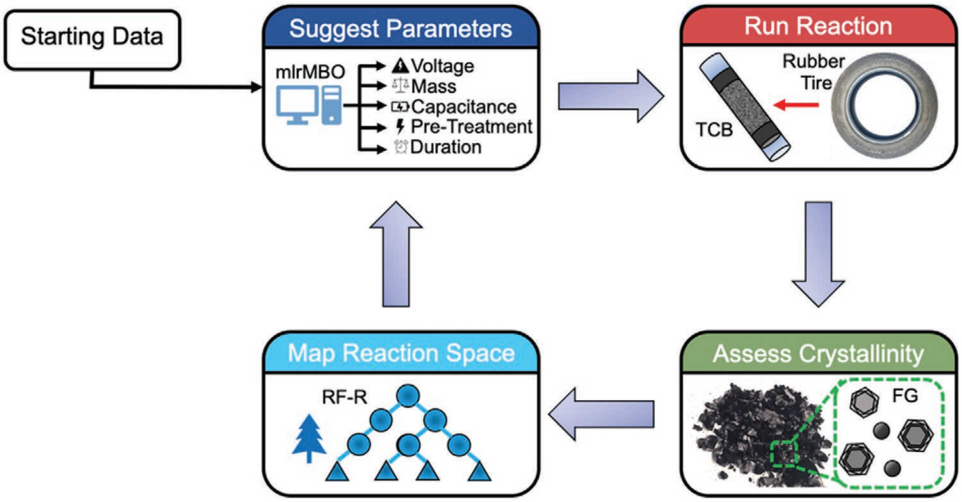

Scheme 1. Scheme showing the feedstock-blind automatic optimization of flash graphene synthesis using a Bayesian meta-learning algorithm.

15214095, 2022, 12, Downloaded from https://onlinelibrary.wiley.com/doi/10.1002/adma.202106506 by Shanxi University, Wiley Online Library on [23/01/2024]. See the Terms and Conditions (https://onlinelibrary.wiley.com/terms-and-conditions) on Wiley Online Library for rules of use; OA articles are governed by the applicable Creative Commons License

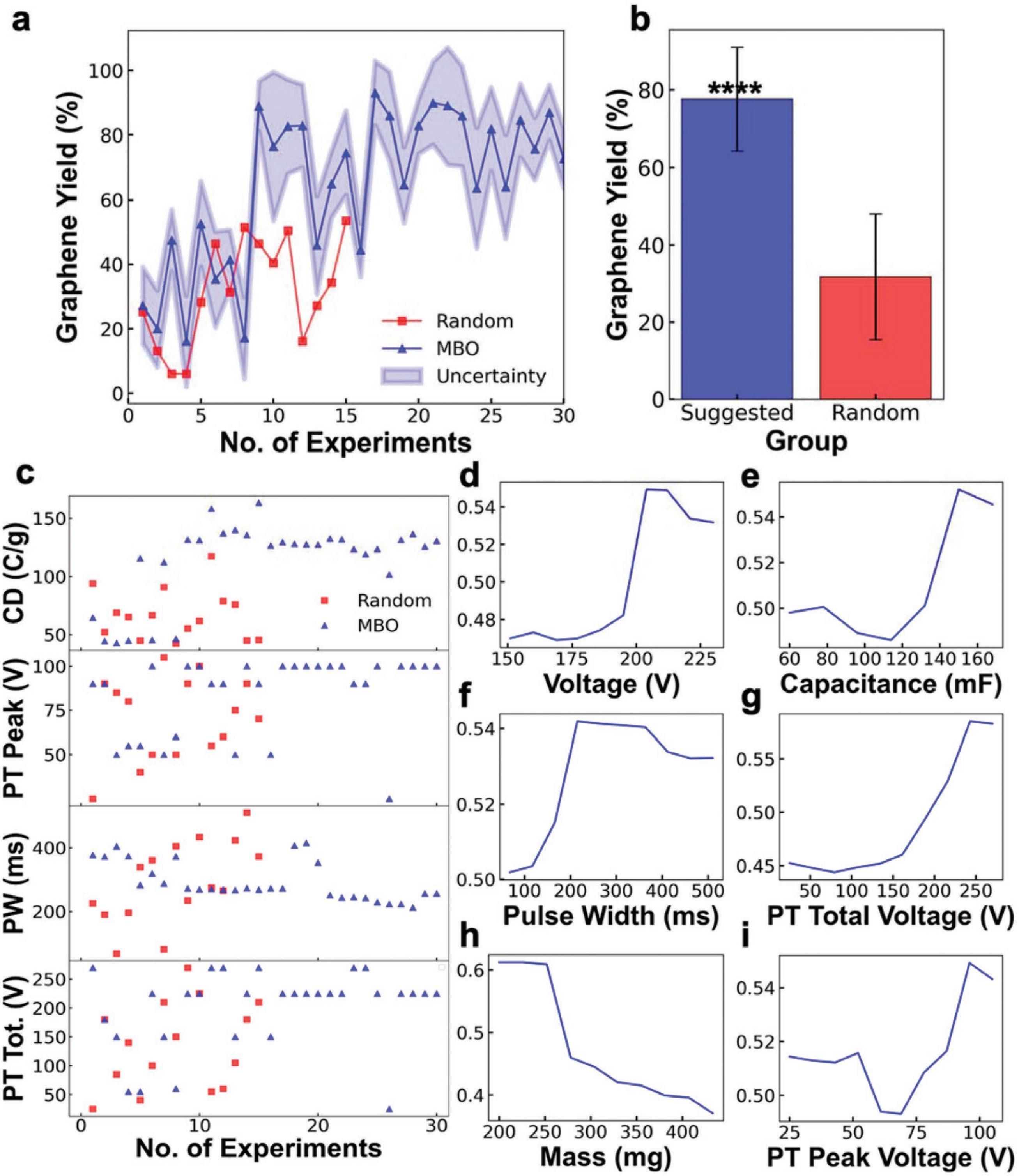

Figure 5. Model-based optimization according to graphene yield. a) Graphene yield of flash Joule heating reactions from tire-derived carbon black using randomized parameters and parameters suggested by a model-based optimization algorithm (MBO). Error bars represent the estimated uncertainty by the algorithm. b) Mean values of the yields given by the randomized parameters and the MBO-suggested parameters. The mean values are different with a significance level of $p < 0.0001$. c) Parameters suggested by the model-based optimization algorithm and random parameters. Mass, voltage, and capacitance are grouped into charge density (CD), calculated as $C \times V/m$. The pretreatment (PT) total voltage, the PT peak voltage, and the pulse width (PW) are also presented. d–i) Partial dependencies of experimental parameters affecting the model-based optimization results, calculated by the RF-R learner algorithm implemented in R.

© 2022 Wiley-VCH GmbH

contributions of starting material properties and the current delivery profile were analyzed. Model-based optimization has been demonstrated to autonomously improve the crystallinity of flash graphene over many trials. These results offer both fundamental insight and practical utility for advancing the use of flash Joule heating in nanomaterials synthesis. We anticipate that the framework laid out in this study can be expanded, potentially via the use of principal component analysis for dimensionality reduction of both the time–current curve and the output Raman spectra. This strategy would allow more advanced ML algorithms to deal directly with collected data, improving accuracy, offering more interpretable conclusions, and streamlining the interplay between ML and flash Joule heating. Overall, the use of ML demonstrates synergy with the flash Joule heating technique, and the continued use of ML models for its study and optimization may maximize its potential for graphene commercialization.

4. Experimental Section

Materials: Four low-or-negative-value feedstocks were employed for conversion to flash graphene: carbon black (Cabot BP2000), metallurgical coke (SunCoke Energy Inc., 70–100 mesh size, 150–210 µm grain size), pyrolysis ash (Shangqiu Zhongming EcoFriendly Equipment Co.), and pyrolyzed rubber tire-derived carbon black (Ergon Asphalt and Emulsion Co.). All materials were ground with a mortar and pestle before and after flash Joule heating but otherwise used as delivered. Commercial graphene nanoplatelets used for comparisons were obtained from XGSciences (xGnP-15, serial #5051209) and used without further modification.

Flash Joule Heating: A custom-built direct-current flash Joule heating station was employed for all experiments. Precursor powders ($100 \leq m \leq 400$ mg) were sandwiched between two graphite electrodes and compressed inside an 8" diameter quartz tube. Then, the samples were placed in a series circuit with ten 6 mF capacitors (Mouser #80-PEH200YX460BQU2) and six 18 mF capacitors (Mouser # 80-ALS70A183QS400). The ten 6 mF capacitors, typically employed for small-scale flash Joule heating reactions in lab, were used as the minimum-size capacitor bank in these experiments, while the six 18 mF capacitors were connected and disconnected from the circuit via circuit breakers to modulate the capacitance employed in each flash reaction. This resulted in C of $60 \text{ mF} \leq C \leq 204$ mF. Voltage to charge the capacitors was supplied by a DC source consisting of an AC wall outlet fed through an AC-DC converter. Samples were subjected to flash Joule heating treatments using a variety of pretreatments, voltages, pulse durations, and reaction atmospheres which are included in the full dataset. Flash Joule heating reactions were conducted inside a desiccator filled with the atmosphere chosen for each reaction. The atmosphere was modulated between argon, CO_2, air, or light vacuum (10 mm Hg), which was not found to have a strong effect on the graphene yield (atmospheres for each individual reaction are tabulated in the full dataset, available on GitHub). The residual voltage after each flash was recorded, resulting in an initial voltage value (V_0) and a voltage drop during flash Joule heating (ΔV) calculated by subtracting the final voltage from the initial voltage. Resistance of the sample was measured before and after each flash to monitor electrical contact between the electrodes and the sample, as well as to assess changes in the conductivity of the carbon products. Mass yields of >80% were typically observed, though this was dependent on the chosen feedstock. Pulse duration was modulated by insulated gate bipolar transistors (IGBTs) with programmable millisecond-level delay time that were connected to a Hall effect sensor through an inductor and controlled via custom LabView scripts. The Hall effect sensor was employed to collect information about current fluctuations over time (time–current curves). These time–current curves were then analyzed via custom-written Python scripts to provide features for the machine learning models.

NOTE: The flash Joule heating reaction employs high voltage with possibility of electric shock or electrocution. See the Supporting Information for a detailed discussion of safety protocols and component selection considerations.

Material Characterization and Analysis: *Raman spectral mapping*: Wide-area Raman spectral mapping was chosen as the principal metric of characterization for this study. Spatial inhomogeneities could bias results obtained from low numbers of sample spectra taken from small areas. Hence, mapping was employed in an area of 1 mm^2, with a minimum of $N = 64$ spectra per map. Spectra were taken with a Renishaw inVia Raman microscope through a 50x lens and using a 5 mW 532 nm Nd:YAG laser for excitation. Renishaw Wire 5.5 LiveTrack software was used to maintain laser focus across large areas. Maps were analyzed via custom-written Python scripts employing the RamPy package.[49] Each of the spectra were baseline-corrected using a RamPy polynomial fit and smoothed using a Savitsky-Golay filter prior to analysis. Each Raman spectrum was classified as either "graphene" or "amorphous carbon" based on I_{2D}/I_G ($I_{2D}/I_G > 0.3$), the FWHM of the 2D band ($15 < \text{FWHM}_{2D} < 70 \text{ cm}^{-1}$), and the signal-to-noise ratio ($\text{SNR}_{2D} > 8$). Spectra without a sufficiently strong G band ($\text{SNR}_G > 8$) were attributed to poor focusing of the laser beam and were not included in the analysis. The "graphene yield" (GY) metric for each sample was calculated as the total number of Raman spectra classified as graphene divided by the total number of Raman spectra taken of that sample, giving an approximate numerical indicator of the sample's bulk crystallinity.

Additional characterization: Scanning electron micrographs were taken with an FEI Helios Nanolab 660 Dual-Beam Scanning Electron Microscope operating in immersion mode and using a through-the-lens detector optimized for high secondary electron yield. Thermogravimetric analysis was conducted using a Q-600 Simultaneous TGA/DSC from TA instruments. A temperature ramp of 10 °C min^{-1} was employed in air. XRD spectra were taken using a Rigaku SmartLab II using a zero-background holder, a scan rate of 8° min^{-1}, and step size of 0.005° per step. X-ray photoelectron spectroscopy was conducted using a PHI Quantera X-ray Scanning Microprobe. C 1s and Auger spectra were collected at a step size of 0.1 eV.

Machine Learning (ML): *ML models*: A total of six different types of ML models (BR, LR, MLP-R, DT-R, RF-R, and XGB-R) were trained to predict graphene yield. All models were constructed directly in Python using the package Scikit-Learn. Models were trained on 80% of the initial dataset and tested on the remaining 20%. Hyperparameter optimization was performed using fivefold cross-validation. Models with variable performance at different random seeds using the train/test split method were trained in five separate instances, and their performance was reported as mean ± standard deviation. Partial dependence was calculated using the Scikit-Learn extension for PD. All data were retained except for flash Joule heating reactions where quartz tubes shattered, resulting in loss of sample. This occurred ≈5% of the time. All data were made publicly available following suggested guidelines.[50]

Feature engineering: Features were empirically selected based on their predictive efficacy in regression models for graphene yield. Five selected features included the charge density (CD), materials type (M), the area under the time–current curve normalized to the mass (A_{IT}), the maximum current value normalized to the mass (I_{max}), and the final current value divided by the maximum current value (I_F/I_{max}).

CD is defined as Equation (1)

$$CD = \frac{V_0 \times C}{m} \tag{1}$$

where V_0 is the voltage, C is the capacitance of the system, and m is the mass of the precursors. M constituted the starting material employed in each flash and was separated using one-hot encoding. A_{IT} was calculated by trapezoidal integration of the discharge curve collected by a Hall effect sensor. As mentioned in the discussion of Figure 3, A_{IT} and CD are conceptually similar quantities with the same units, but they convey different information about the system. The calculation of CD used the

© 2022 Wiley-VCH GmbH

15214095, 2022, 12, Downloaded from https://onlinelibrary.wiley.com/doi/10.1002/adma.202106506 by Shanxi University, Wiley Online Library on [23/01/2024]. See the Terms and Conditions (https://onlinelibrary.wiley.com/terms-and-conditions) on Wiley Online Library for rules of use; OA articles are governed by the applicable Creative Commons License

initial voltage V_0. By contrast, measurement of A_{IT} was depended on the voltage drop during the reaction ΔV. V_0 and ΔV were different values because complete discharge was rare in the flash Joule heating reactions run in this study. They differed by the value of the residual voltage. An alternative version of CD was constructed using the voltage drop ΔV instead of the initial voltage V_0, but this metric was less predictive of crystallinity (Table S2, Supporting Information) and correlated strongly with A_{IT} (Pearson's correlation coefficient of $r = 0.85$).

I_{Max} was calculated as the maximum current recorded in the discharge divided by the mass. I_F/I_{Max} was calculated as the final recorded current in the flash divided by the maximum current. A visual depiction of how each of the time–current curve-derived features were calculated can be found in Figure 3a. The five selected features were empirically chosen based on their ability to improve model performance. Other features attempted are tabulated in Table S2 in the Supporting Information. These features were not included in the final model for one of two reasons: i) decreased model performance or ii) high correlation with existing features.

Evaluation metrics: All regression evaluation metrics were calculated using existing Scikit-Learn plugins. The r^2 score was chosen as the principal metric due to its ability to compare model performance over a performance baseline (a model that predicted the mean output value for every sample). The r^2 score was defined as Equation (2)

$$r^2 = 1 - \frac{\sum_{i=1}^{n} (y_i - \hat{y}_i)^2}{\sum_{i=1}^{n} (y_i - \overline{y}_i)^2} \tag{2}$$

where y_i is the true value of each sample, $\hat{y}_i$ is the value predicted by the model, and $\overline{y}_i$ is the mean output value. RMSE values were also reported.

Data inclusion: At the spectra-level, all spectra identified as having a G peak (a maximum in the range of $1500\ \text{cm}^{-1} < x < 1700\ \text{cm}^{-1}$ with an SNR of >8) were included in the analysis. Spectra not containing a G peak were attributed to poor laser focusing. At the individual sample level, all samples with >64 viable spectra, a properly recorded accompanying current/time profile, and which did not cause an explosion of the quartz tube were included in the analysis.

Bayesian Optimization: Bayesian model-based optimization was implemented in R using the package mlrMBO.[51] Graphene yield (GY) was defined as the objective function, and the sample pretreatment, voltage, pulse time, mass, and capacitance of the flash Joule heating reaction were defined as the inputs. All experiments were performed with carbon derived from pyrolyzed rubber tires. The default RF-R with 500 trees was defined as the surrogate model. Since the number of experiments was low ($N = 30$), the acquisition function was modulated between the expected improvement (EI) and augmented expected improvement (AEI) functions in a human-in-the-loop configuration to encourage exploration of the parameter space.

Supporting Information

Supporting Information is available from the Wiley Online Library or from the author.

Acknowledgements

This work was supported by the funding from The Air Force Office of Scientific Research (FA9550-19-1-0296), U.S. Army Corps of Engineers, ERDC (W912HZ-21-2-0050), and the DOE-NETL (DE-FE0031794). The authors thank Ergon Asphalt and Emulsions, Inc. for providing the rubber-tire-derived carbon black material, SunCoke Energy Inc. for providing the metallurgical coke, and Shangqiu Zhongming EcoFriendly Equipment Co. for providing the plastic waste-derived pyrolysis ash. J.L.B. and K.M.W. acknowledge the National Science Foundation Graduate Research Fellowship Program for financial support. The authors acknowledge the use of equipment under the jurisdiction of the Rice University Shared Equipment Authority and the Electron Microscopy Center. J.L.B. acknowledges support from the National Science Foundation (award number: 1825352) and the United States National Energy Technology Laboratory (DE-FE0031645). The authors thank Allison Kaczmarek (Massachusetts Institute of Technology) and Mikita Misiura (Rice University) for useful help and discussion.

Conflict of Interest

The flash graphene synthesis process is the intellectual property of Rice University. J.M.T. is a stockholder in Universal Matter Ltd., a company licensing the flash graphene intellectual property of Rice University but is not serving as an officer or director. All conflicts of interest are managed through regular disclosure to the Rice University Office of Sponsored Programs and Research Compliance.

Author Contributions

J.L.B. designed the study, constructed the ML models, assisted K.M.W. with dataset construction, and wrote the manuscript. K.M.W. constructed most of the dataset and helped with additional characterization. Y.X. assisted J.L.B. with the construction of the ML models, under the guidance of J.L. E.A.M. collected thermograms of flash graphene and assisted with the writing of the manuscript. J.T.L. collected scanning electron micrographs of flash graphene. P.A.A. assisted with the construction of an initial dataset. W.C. assisted with the material characterization and guided experiments that were used to validate conclusions about the role of the starting material. All aspects of the research were overseen by J.M.T.

Data Availability Statement

The data that support the findings of this study are available from the corresponding author upon reasonable request.

Keywords

flash graphene, flash Joule heating, machine learning, nanomanufacturing

Received: August 18, 2021
Revised: December 15, 2021
Published online: February 10, 2022

---

[1] D. X. Luong, K. V. Bets, W. A. Algozeeb, M. G. Stanford, C. Kittrell, W. Chen, R. V. Salvatierra, M. Ren, E. A. McHugh, P. A. Advincula, Z. Wang, M. Bhatt, H. Guo, V. Mancevski, R. Shahsavari, B. I. Yakobson, J. M. Tour, *Nature* **2020**, *577*, 647.
[2] N. Gupta, S. Walia, U. Mogera, G. U. Kulkarni, *J. Phys. Chem. Lett.* **2020**, *11*, 2797.
[3] U. Mogera, R. Dhanya, R. Pujar, C. Narayana, G. U. Kulkarni, *J. Phys. Chem. Lett.* **2015**, *6*, 4437.
[4] W. Chen, Z. Wang, K. V. Bets, D. X. Luong, M. Ren, M. G. Stanford, E. A. McHugh, W. A. Algozeeb, H. Guo, G. Gao, B. Deng, J. Chen, J. T. Li, W. T. Carsten, B. I. Yakobson, J. M. Tour, *ACS Nano* **2021**, *15*, 1282
[5] Y. Yao, Z. Huang, P. Xie, S. D. Lacey, R. J. Jacob, H. Xie, F. Chen, A. Nie, T. Pu, M. Rehwoldt, D. Yu, M. R. Zachariah, C. Wang, R. Shahbazian-Yassar, J. Li, L. Hu, *Science* **2018**, *359*, 1489.

© 2022 Wiley-VCH GmbH

15214095, 2022, 12, Downloaded from https://onlinelibrary.wiley.com/doi/10.1002/adma.202106506 by Shanxi University, Wiley Online Library on [23/01/2024]. See the Terms and Conditions (https://onlinelibrary.wiley.com/terms-and-conditions) on Wiley Online Library for rules of use; OA articles are governed by the applicable Creative Commons License

[6] Z. Huang, Y. Yao, Z. Pang, Y. Yuan, T. Li, K. He, X. Hu, J. Cheng, W. Yao, Y. Liu, A. Nie, S. Sharifi-Asl, M. Cheng, B. Song, K. Amine, J. Lu, T. Li, L. Hu, R. Shahbazian-Yassar, *Nat. Commun.* **2020**, *11*, 6373.

[7] W. Chen, J. T. Li, Z. Wang, W. A. Algozeeb, D. X. Luong, C. Kittrell, E. A. McHugh, P. A. Advincula, K. M. Wyss, J. L. Beckham, M. G. Stanford, B. Jiang, J. M. Tour, *ACS Nano* **2021**, *15*, 11158.

[8] P. A. Advincula, D. X. Luong, W. Chen, S. Raghuraman, R. Shahsavari, J. M. Tour, *Carbon* **2021**, *178*, 649.

[9] K. M. Wyss, J. L. Beckham, W. Chen, D. X. Luong, P. Hundi, S. Raghuraman, R. Shahsavari, J. M. Tour, *Carbon* **2021**, *174*, 430.

[10] W. A. Algozeeb, P. E. Savas, D. X. Luong, W. Chen, C. Kittrell, M. Bhat, R. Shahsavari, J. M. Tour, *ACS Nano* **2020**, *14*, 15595.

[11] P. Narang, C. A. C. Garcia, C. Felser, *Nat. Mater.* **2020**, *1*, 293.

[12] K. T. Butler, D. W. Davies, H. Cartwright, O. Isayev, A. Walsh, *Nature* **2018**, *559*, 547.

[13] Y. Zhang, C. Ling, *npj Comput. Mater.* **2018**, *4*, 25.

[14] Y. Dong, C. Wu, C. Zhang, Y. Liu, J. Cheng, J. Lin, *npj Comput. Mater.* **2019**, *5*, 26.

[15] Y. Dong, D. Li, C. Zhang, C. Wu, H. Wang, M. Xin, J. Chang, J. Lin, *Carbon* **2020**, *169*, 9.

[16] B. Tang, Y. Lu, J. Zhou, T. Chouhan, H. Wang, P. Golani, M. Xu, Q. Xu, C. Guan, Z. Liu, *Mater. Today* **2020**, *41*, 72.

[17] Y. Xie, C. Zhang, X. Hu, C. Zhang, S. P. Kelley, J. L. Atwood, J. Lin, *J. Am. Chem. Soc.* **2020**, *142*, 1475.

[18] K.-H. Tu, H. Huang, S. Lee, W. Lee, Z. Sun, A. Alexander-Katz, C. A. Ross, *Adv. Mater.* **2020**, *32*, 2005713.

[19] K. A. Brown, S. Brittman, N. Maccaferri, D. Jariwala, U. Celano, *Nano Lett.* **2020**, *12*, 2.

[20] E. Samaniego, C. Anitescu, S. Goswami, V. M. Nguyen-Thanh, H. Guo, K. Hamdia, X. Huang, T. Rabczuk, *Comput. Methods Appl. Mech. Eng.* **2020**, *362*, 112790.

[21] C. Anitescu, E. Atroshchenko, N. Alajlan, T. Rabczuk, *Comput. Mater. Continua* **2019**, *59*, 345.

[22] M. Zhong, K. Tran, Y. Min, C. Wang, Z. Wang, C.-T. Dinh, P. D. Luna, Z. Yu, A. S. Rasouli, P. Brodersen, S. Sun, O. Voznyy, C.-S. Tan, M. Askerka, F. Che, M. Liu, M. Seifitokaldani, Y. Pang, S.-C. Lo, A. Ip, Z. Ulissi, E. H. Sargent, *Nature* **2020**, *581*, 178.

[23] H. Wahab, V. Jain, A. S. Tyrrell, M. A. Seas, L. Kotthoff, P. A. Johnson, *Carbon* **2020**, *167*, 609.

[24] K. Terayama, M. Sumita, R. Tamura, K. Tsuda, *Acc. Chem. Res.* **2021**, *54*, 1334.

[25] D. Salley, G. Keenan, J. Grizou, A. Sharma, S. Martín, L. Cronin, *Nat. Commun.* **2020**, *11*, 2771.

[26] A. E. Gongora, B. Xu, W. Perry, C. Okoye, P. Riley, K. G. Reyes, E. F. Morgan, K. A. Brown, *Sci. Adv.* **2020**, *6*, 1708.

[27] J. M. Granda, L. Donina, V. Dragone, D.-L. Long, L. Cronin, *Nature* **2018**, *559*, 377.

[28] K. Terayama, M. Sumita, R. Tamura, D. T. Payne, M. K. Chahal, S. Ishihara, K. Tsuda, *Chem. Sci.* **2020**, *11*, 5959.

[29] A. C. Ferrari, *Solid State Commun.* **2007**, *143*, 47.

[30] L. M. Malard, M. A. Pimenta, G. Dresselhaus, M. S. Dresselhaus, *Phys. Rep.* **2009**, *473*, 51.

[31] A. C. Ferrari, D. M. Basko, *Nat. Nanotechnol.* **2013**, *8*, 235.

[32] J. A. Garlow, L. K. Barrett, L. Wu, K. Kisslinger, Y. Zhu, J. F. Puleczio, *Sci. Rep.* **2016**, *6*, 19804.

[33] I. Kruglov, O. Sergeev, A. Yanilkin, A. R. Oganov, *Sci. Rep.* **2017**, *7*, 8512.

[34] T. Yamashita, N. Sato, H. Kino, T. Miyake, K. Tsuda, T. Oguchi, *Phys. Rev. Mater.* **2018**, *2*, 013803.

[35] S. Jaeger, S. Fulle, S. Turk, *J. Chem. Inf. Model.* **2018**, *58*, 27.

[36] M. Ture, F. Tokatli, I. Kurt, *Expert Syst. Appl.* **2009**, *36*, 2017.

[37] F. Pedregosa, G. Varoquaux, A. Gramfort, V. Michel, B. Thirion, O. Grisel, M. Blondel, P. Prettenhofer, R. Weiss, V. Dubourg, J. Vanderplas, A. Passos, D. Cournapeau, *J. Mach. Learn. Res.* **2011**, *12*, 2825.

[38] T. Chen, C. Guestrin in Proc. 22nd ACM SIGKDD Int. Conf. Knowledge Discovery and Data Mining, ACM, San Francisco, CA 2016, pp. 785–794.

[39] Y. Han, B. Tang, L. Wang, H. Bao, Y. Lu, C. Guan, L. Zhang, M. Le, Z. Liu, M. Wu, *ACS Nano* **2020**, *14*, 14761.

[40] M. Ryo, M. C. Rillig, *Ecosphere* **2017**, *8*, e01976.

[41] P. J. F. Harris, *Carbon* **2017**, *122*, 504.

[42] K. S. Ravi Chandran, *Int. J. Heat Mass Transfer* **2015**, *88*, 14.

[43] J. Y. Huang, S. Chen, Z. F. Ren, G. Chen, M. S. Dresselhaus, *Nano Lett.* **2006**, *6*, 1699.

[44] L. X. Duy, Z. Peng, Y. Li, J. Zhang, Y. Ji, J. M. Tour, *Carbon* **2018**, *126*, 472.

[45] M. G. Stanford, K. V. Bets, D. X. Luong, P. A. Advincula, W. Chen, J. T. Li, Z. Wang, E. A. McHugh, W. A. Algozeeb, B. I. Yakobson, J. M. Tour, *ACS Nano* **2020**, *14*, 13691.

[46] N. T. K. Thanh, N. Maclean, S. Mahiddine, *Chem. Rev.* **2014**, *114*, 7610.

[47] R. W. Epps, M. S. Bowen, A. A. Volk, K. Abdel-Latif, S. Han, K. G. Reyes, A. Amassian, M. Abolhasani, *Adv. Mater.* **2020**, *32*, 2001626.

[48] J. L. E. Campos, H. Miranda, C. Rabelo, E. Sandoz-Rosado, S. Pandey, J. Riikonen, A. G. Cano-Marquez, A. Jorio, *J. Raman Spectrosc.* **2018**, *49*, 54.

[49] C. L. Losq, *Rampy: A Python Library for Processing Spectroscopic (IR, Raman, XAS) Data*, Zenodo, Switzerland **2018**.

[50] N. Artrith, K. T. Butler, F.-X. Coudert, S. Han, O. Isayev, A. Jain, A. Walsh, *Nat. Chem.* **2021**, *13*, 505

[51] B. Bischl, J. Richter, J. Bossek, D. Horn, J. Thomas, M. Lang mlrMBO: A Modular Framework for Model-Based Optimization of Expensive Black-Box Functions, 2017 (accessed: January **2022**) https://arxiv.org/abs/1703.03373.

© 2022 Wiley-VCH GmbH

15214095, 2022, 12, Downloaded from https://onlinelibrary.wiley.com/doi/10.1002/adma.202106506 by Shanxi University, Wiley Online Library on [23/01/2024]. See the Terms and Conditions (https://onlinelibrary.wiley.com/terms-and-conditions) on Wiley Online Library for rules of use; OA articles are governed by the applicable Creative Commons License